ACS SENSORS

pubs.acs.org/acssensors

Article

Transcutaneous Flexible Sensor for *In Vivo* Photonic Detection of pH and Lactate

Dat Nguyen, Micah M. Lawrence, Haley Berg, Monika Aya Lyons, Samir Shreim, Mark T. Keating, John Weidling, and Elliot L. Botvinick*

Cite This: *ACS Sens.* 2022, 7, 441−452

Read Online

ACCESS | Metrics & More | Article Recommendations | Supporting Information

ABSTRACT: Clinical research shows that frequent measurements of both pH and lactate can help guide therapy and improve patient outcome. However, current methods of sampling blood pH and lactate make it impractical to take readings frequently (due to the heightened risk of blood infection and anemia). As a solution, we have engineered a subcutaneous pH and lactate sensor (PALS) that can provide continuous, physiologically relevant measurements. To measure pH, a sheet containing a pH-sensitive fluorescent dye is placed over 400 and 465 nm light-emitting diodes (LEDs) and a filter-coated photodetector. The filter-coated photodetector collects an emitted signal from the dye for each LED excitation, and the ratio of the emitted signals is used to monitor pH. To measure lactate, two sensing sheets comprising an oxygen-sensitive phosphorescent dye are each mounted to a 625 nm LED. One sheet additionally comprises the enzyme lactate oxidase. The LEDs are sequentially modulated to excite the sensing sheets, and their phase shift at the LED drive frequency is used to monitor lactate. *In vitro* results indicate that PALS successfully records pH changes from 6.92 to 7.70, allowing for discrimination between acidosis and alkalosis, and can track lactate levels up to 9 mM. Both sensing strategies exhibit fast rise times (< 5 min) and stable measurements. Multianalyte *in vitro* models of physiological disorders show that the sensor measurements consistently quantify the expected pathophysiological trends without cross talk; *in vivo* rabbit testing further indicates usefulness in the clinical setting.

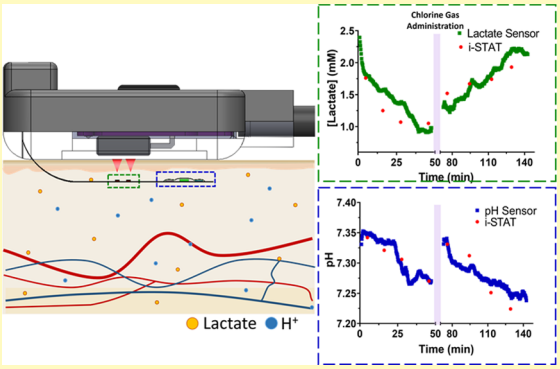

KEYWORDS: *pH sensor, lactate sensor, multianalyte, photonic, continuous monitoring, critical care monitoring*

pH and lactate are biomarkers that can be monitored during sepsis and liver and lung disease to improve patient outcome.[1−4] Blood pH is naturally buffered to within a range of 7.35 to 7.45 and deviations from this range can be indicative of serious disease.[4,5] Examples of these deviations are in cases of metabolic acidosis and alkalosis where blood pH can change when the body has too high or low concentration of hydrogen ions (H^+) and/or bicarbonate.[4,5] A form of metabolic acidosis is lactic acidosis, which can occur when lactate is generated in excess (hyperlactatemia, >2 mM) and the amount of circulating H^+ exceeds the capacity of the blood's buffering system.[6,7] Elevated lactate levels are often a sign of cellular hypoxia as lactate is excessively produced during anaerobic glycolysis.[8] An increase in lactate can result in a decrease in pH; however, this is not always the case. For this reason, it is important to recognize that measuring only lactate or pH is not a surrogate for measuring the other. For example, in respiratory acidosis, pH may be directly influenced by an accumulation of carbon dioxide in the blood, while lactate remains unchanged.[9] In this case, frequent pH measurements can guide therapy. Importantly, there are a variety of circumstances when both pH and lactate should be measured simultaneously. Frequently referenced examples are during sepsis or septic shock as Lee et al. found that both the lactate levels and pH are essential when predicting patient mortality.[1]

Current clinical standards for measuring blood pH and lactate require intermittent blood draws and analysis using benchtop instruments (Yellow Springs Instrument, YSI) or hand-held monitors (Abbott Laboratories i-STAT).[10−12] The frequency of measurements is limited ultimately by the frequency of blood draws which increase the likelihood of blood infections and anemia.[10,13] Meanwhile, there is substantial evidence suggesting that attentive monitoring and treatment of pH and lactate can improve patient prognosis and outcome.[14,15] In a multisite study with 348 patients having initial lactate ≥3.0 mEq/L, goal-oriented treatment targeting a 10% decrease in lactate per hour increased patient survivability

Received: August 12, 2021
Accepted: January 31, 2022
Published: February 17, 2022

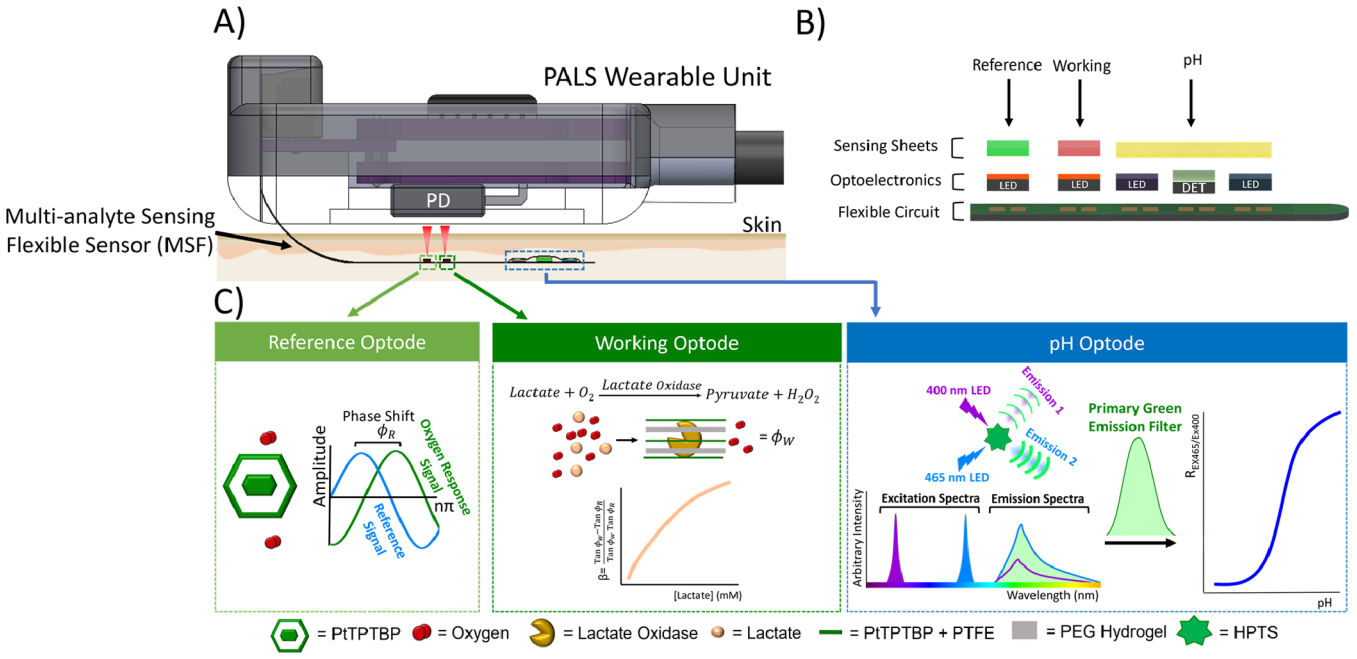

Figure 1. Schematic overview of PALS. (A) PALS comprises a wearable unit and a transcutaneous multianalyte sensing flexible (MSF) Sensor for pH and lactate monitoring. (B) Exploded view of the MSF tip. LEDs and the detector (DET) are soldered onto conductive pads of the flexible circuit. Sensing sheets are adhered to their corresponding optoelectronic components. The green bar above DET indicates the color filter. (C) (left) Oxygen is monitored by analyzing the PtTPTBP light emission phase shift using a photodetector (PD) housed in the wearable unit. (middle) Lactate oxidase consumes both oxygen and lactate; oxygen consumption can be used as an indirect measurement of lactate. (right) pH is measured by ratiometric analysis of HPTS light emission.

by 10% as compared to the control (standard treatment, $p = 0.067$).[16] In addition to reduced mortality, patients were discharged from the intensive care unit (ICU) earlier than those in the control group. Moreover, in a prospective study with 75 patients experiencing sepsis and metabolic acidosis, both pH and lactate endpoint values were concluded as vital biomarkers toward patient outcome.[17] In this study, the 11 nonsurvivors had a lower mean pH and a higher mean lactate level than survivors after 5 days in the ICU. Changes in pH and lactate were not statistically significant ($p > 0.714$) as compared to initial values for the nonsurvivors, whereas significant changes were observed for the 64 survivors ($P < 0.002$).[17] Monitoring pH and lactate clearly has major implications toward patient prognosis, underscoring the value of a continuous pH and lactate sensor.

There are well-established pH sensing modalities including electrochemical-based electrodes and luminescent dyes. Electrochemical-based glass and metal oxide electrodes measure pH through a difference in H^+ concentration between a sensitive and reference electrode.[18,19] Although glass electrodes provide the highest level of specificity, they cannot be easily miniaturized and require frequent calibration.[19] Metal oxide electrodes can be easily miniaturized but exhibit low resolution, large drift, and hysteresis.[18,20] Meanwhile, pH-sensitive luminescent probes vary in their linear range of sensitivity (pK_a), quantum yield, and mode of operation (intensity, emission ratio, etc.).[21−24] To continuously monitor pH on a transcutaneous sensor, we have selected luminescent dye 8-hydroxypyrene-1,3,6-trisulfonic acid trisodium salt (HPTS). HPTS has a reported pK_a of 7.3 and exhibits minimal toxicity, a quantum yield of 0.82 in water, and a linear response ranging from 6.7 to 8.7, which spans the pathophysiological range of acidosis and alkalosis.[25,26] HPTS peak emission intensity at 520 nm is a function of its spectral absorption efficiency. HPTS absorbs light more efficiently at 450 nm at high pH as compared to low pH. Conversely, HTPS absorbs 405 nm light more efficiently at lower pH values.[27] It has been shown that with serial light excitation at 450 and 405 nm, HPTS can reliably measure pH through a ratiometric analysis at its peak emission wavelength.[27,28] In an approach similar to our own, Wencel et al. immobilized HPTS in a sol−gel placed at the tip of a multicore fiber and calibrated pH to the ratio of 520 nm emission with dual LED excitation.[29]

Numerous strategies exist to measure lactate, including colorimetric assays, high-performance liquid chromatography, and enzyme-linked immunosorbent assays.[30−32] One common mode of enzyme-based lactate sensing (as used in the YSI 2300 STAT Plus Glucose and Lactate Analyzer) employs lactate oxidase (LOX).[33] The LOX reaction consumes both oxygen and lactate while producing hydrogen peroxide and pyruvate. This allows lactate to be indirectly measured through monitoring the consumption of oxygen or generation of hydrogen peroxide.[30,31] The generation of hydrogen peroxide is commonly used for electrochemical-based LOX sensing of lactate.[33−35] Common challenges in such electrochemical sensing include high operation voltages, dependencies on electron-transfer mediators (which can be toxic and exhibit poor solubility), and acetaminophen interference.[34,36,37] As an alternative to electrochemical sensing, our group and others have published the use of a phosphorescent oxygen-sensitive dye for continuous measurements of lactate and other analytes.[38,39] In our clinical studies, oxygen was detected by the metalloporphyrin dye platinum(II) meso-tetraphenyl tetrabenzoporphine (PtTPTBP).[39] PtTPTBP phosphorescence is quenched by oxygen, reducing its luminescence lifetime. This lifetime can be assessed by determining the phase

https://doi.org/10.1021/acssensors.1c01720
ACS Sens. 2022, 7, 441−452

shift between excitation and emission waveforms.[40] An indirect measurement of lactate may therefore be reported by calculating the phase shift of PtTPTBP emission in the presence of LOX, lactate, and oxygen. This sensing scheme is adapted here to continuously monitor lactate within a multianalyte sensor.

Herein, we introduce a transcutaneous, continuous multianalyte sensor referred to as the PALS (Figure 1A). PALS employs two unique sensing modalities at the tip of a transcutaneous multianalyte sensing flexible (MSF) Sensor to monitor pH and lactate: (1) a dual excitation, single-band detection scheme that collects pH-sensitive light emissions and (2) a luminescence lifetime detection scheme that captures oxygen and lactate-sensitive light emissions (Figure 1B). PALS *in vitro* results show rapid rise time for both pH and lactate sensing, measurement reversibility, and sensitivity across their respective pathophysiological ranges. Furthermore, when measuring both analytes simultaneously, measurements were shown to be free of cross talk. An implant study in a rabbit model of hypoxemia provides further evidence that PALS signals are reversible and in agreement with reference values from a handheld blood gas analyzer. The ability of PALS to optically measure pH and lactate using a transcutaneous sensor contributes to the novelty of our technology and provides an advantage over electrochemical sensors which are prone to chemical species interference.

METHODS

Filter-Coated Photodetector. For the pH sensor, silicon photodiodes (PDs) were coated with an optical filter as follows. A plastic green bandpass filter (Primary Green Filter, Lee filters, USA) was first cut into a 2 cm × 2 cm square. The square filter was then placed onto the surface of a 2 mm × 1.25 mm silicon PD (SFH2716, OSRAM Opto Semiconductors, Germany) that had been mounted on a microscope glass slide. The edges of the filter were held in place by two additional glass slides. A Varitemp VT-750C heat gun (Master Appliance, USA) at a temperature setting of 250°C was then used to melt the plastic green bandpass filter onto the PD (Figure S1).

pH Sensor Sheet. First, a 12.7 mM HPTS stock solution was formulated by dissolving 99 mg of HPTS (MilliporeSigma, USA) in 15 mL of Milli-Q water (MilliporeSigma, 18.2 MΩ·cm at 25 °C). A total of 10 g of 45−150 μm diameter Dowex 1X8 resin beads (MilliporeSigma, USA) was then suspended in the stock solution within a 20 mL disposable scintillation vial. This process yields the resin bead suspension (Figure 2A) and allows the negatively charged sulfonate groups on HPTS to ionically bind to the positively charged Dowex Resin.[25] A total of 500 μL of the resin bead suspension was then added to a 1.5 mL amber glass vial along with 50 mg of poly(ethylene glycol) dimethacrylate 8000 (PEGDMA8000, Polysciences, USA) and 12 mg of 2-hydroxy-1-(4-(2-hydroxyethoxy)-phenyl)-2-methylpropan-1-one (Irgacure 2959, Sigma-Aldrich, USA), creating the pH sensor suspension (Figure 2B). PEGDMA is considered a biocompatible material with applications including drug delivery and cell encapsulation.[41−43]

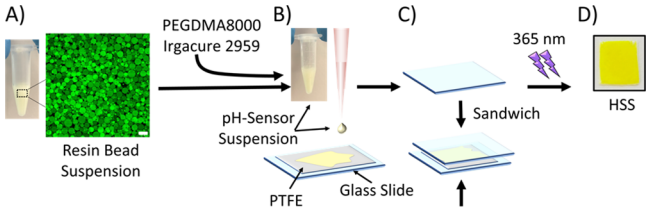

Figure 2. HSS Fabrication. (A) Fluorescence confocal micrograph (Olympus Fluoview 1200) of the pH-sensitive resin bead suspension (405 nm laser excitation, emission bandpass filter: 505−540 nm). Scale bar = 100 μm. (B) Suspension is pipetted onto a PTFE sheet. (C) Suspension is sandwiched between two glass slides. (D) Suspension is polymerized, yielding the HSS. The HSS is hydrated to allow for hydrogel swelling.

To fabricate the pH sensor sheet (HSS), a thin circular sheet of hydrophilic polytetrafluoroethylene (PTFE, H050A047A, 35 μm thick, 0.50 μm pores, 47 mm diameter, Sterlitech, USA) was cut into a 1.2 cm × 1 cm rectangle and placed onto a microscope glass slide. PTFE was chosen as the sensing film substrate because PTFE is biocompatible and is commonly used in dwelling commercial insulin infusion cannulas.[44−48] A total of 40 μL of the pH sensor suspension was then pipetted onto the cut PTFE sheet. The sheet was then sandwiched between two glass slides (Figure 2C) until the pH sensor suspension uniformly coated one side of the sheet. The pores of the PTFE sheet are 2 orders of magnitude smaller than the resin bead diameter, preventing resin penetration into the sheet. The coated sheet was then polymerized for 15 min using 365 nm wavelength light emitted from an 8 W dual-ultraviolet (UV) transilluminator (VWR, USA) to produce the HSS (Figure 2D). Upon UV polymerization, the resin bead suspension is encapsulated within a PEGDMA network that also polymerizes throughout the porous network of the PTFE. Thus, all materials in contact with the tissue are known to be biocompatible, nontoxic, and nonfouling.[49] To test for HPTS leaching out of the HSS, HSSs were incubated in 200 μL of PBS for 8 days. Absorption of 405 nm light in the incubation solution was measured in triplicate using a spectrophotometer (NanoDrop OneC, Thermo Scientific). Standards were formulated at concentrations 12.7 × [10^{0} 10^{1} 10^{-2} 10^{-3} 10^{-4} 10^{-5}] mM HPTS. All but the 12.7 × 10^{-5} mM HPTS solution had detectable absorption. Neither the HSS sample nor a negative control HSS lacking HPTS had detectable absorption, indicating negligible leaching over the 8 days. The HSS was then retrieved with tweezers and left to swell for at least 2 h in Milli-Q water within a 20 mL scintillation vial.

LOX and Oxygen Sensor Sheets. LOX sheets were fabricated from PTFE sheets coated with the oxygen-sensitive dye, the protein mixture containing enzymes LOX and catalase, and pretreatment solution, all of which are detailed in the Supporting Information. First, a 1 cm × 1 cm square of the dye-coated PTFE sheet was excised using a razor blade. A total of 4.5 μL of pretreatment solution was then pipetted onto each of the two microscope glass slides (Figure 3A).

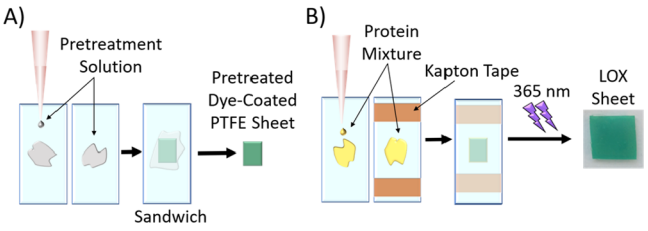

Figure 3. LOX sheet fabrication. (A) Pretreatment solution wets the dye-coated PTFE sheet. (B) Pretreated dye-coated PTFE sheet is sandwiched between glass slides containing the protein mixture. Strips of Kapton tape serve as spacers to control the membrane thickness. UV polymerization cures the LOX sheet.

Next, the dye-coated PTFE sheet was sandwiched between the two glass slides to force the pretreatment solution into the pores of the sheet. The purpose of the pretreatment solution is to establish a porous network within the dye-coated PTFE sheet that limits the diffusion of lactate and oxygen. Next, two parallel double-layered strips of 25 μm-thick Kapton tape (Tapes Master, USA) were applied to a glass slide to function as spacers. A total of 4.5 μL of protein mixture was then pipetted in between the spacers and onto a second slide. The pretreated dye-coated PTFE sheet was then placed between the spacers and sandwiched between the glass slides. While being sandwiched, the sensor sheet was polymerized with the 8 W dual-UV transilluminator for 5 min to yield the LOX sheet (Figure 3B). The

https://doi.org/10.1021/acssensors.1c01720
ACS Sens. 2022, 7, 441−452

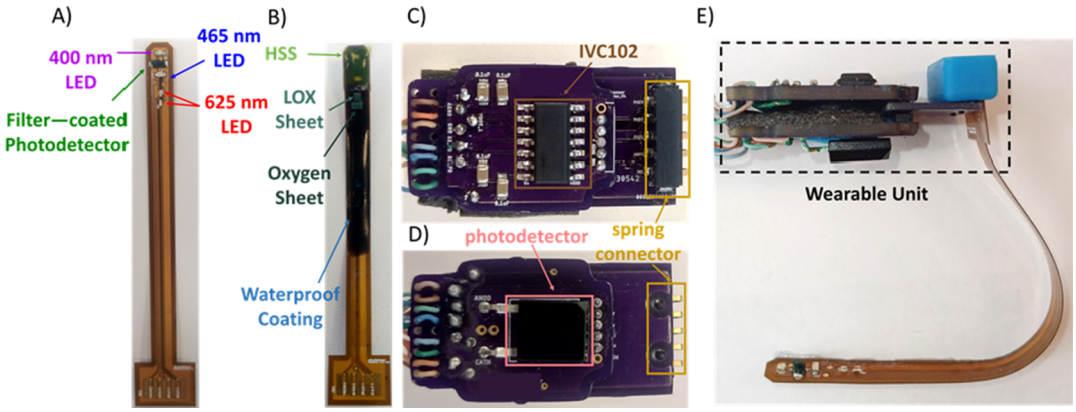

Figure 4. PALS sensing components. (A) MSF containing five on-strip optoelectronic components required for sensing. (B) Fully assembled MSF comprising sensing sheets and waterproof coating. (C) Integrator board for amplifying pH signals. (D) Photodetector board for lactate and oxygen sensing. (E) PALS wearable unit connected to the MSF.

oxygen sheet was fabricated in a similar fashion except for the exclusion of LOX and catalase in its protein mixture.

PALS Circuitry. PALS consists of custom-made printed circuit boards (fabricated by OSH Park, USA) designed using Eagle (Autodesk, USA). Essential components of the circuits are shown in Figure S2. These custom boards were manually assembled and make up the three main subunits of PALS. The first subunit is the MSF (Figure 4A). The second subunit is the wearable unit comprising three circuit boards: (1) the integrator board for pH sensing that utilizes an IVC102 transimpedance amplifier (Texas Instruments, USA, Figure 4C), (2) the photodetector board for lactate and oxygen sensing (Figure 4D), and (3) the connector board to connect the photodetector and integrator boards to the MSF (Figure 4E). The last subunit is the backend controller unit (shown in Figure S2) comprising a microcontroller Teensy 3.2 (PJRC, USA) and two circuit boards: (1) the controller board for charlieplexing and tuning the drive current of the MSF LEDs (Figure S2A) and (2) the IVC power supply board. Custom software was written for Teensy 3.2 to charlieplex the LEDs and acquire data, using a combination of Arduino (Arduino, USA) with Teensyduino library (PJRC, USA) and LabView (National Instruments, USA).

Custom-designed housings were printed using a stereolithography printer (Prusa SL1, Prusa Research, Czech Republic) to protect and house the wearable unit, as illustrated in Figure 1. The housing unit serves to also pressure-connect the prongs of the 5-spring battery connector (009155005852006, AVX Corporation, USA) on the connector board to the gold pads of the MSF, as depicted in Figure 4E.

MSF Fabrication. The MSF was printed and designed with OSH Park and Eagle. The MSF comprises polyimide, which exhibits insignificant cytotoxicity and protein adsorption when compared to PTFE and polydimethylsiloxane.[50,51] The MSF contains optoelectronic components for both pH and lactate sensing (Figure 4A). The optoelectronic components for pH sensing are a 400 nm LED (SM0603UV-400, Bivar, USA), a 465 nm LED (APT1608QBC/G, Kingbright, USA), and a filter-coated photodetector. Two 625 nm LEDs (APHHS1005LSECK/J3-PF, Kingbright, USA) are used for lactate and oxygen sensing. The flex circuit is 0.135 mm thick, the detector is 0.8 mm tall, and the pH sensing sheet is 0.035 μm thick. Collectively, the thickest portion of MSF is 1.15 mm. Each LED spectrum is shown in Figure S3. Additionally, Video S1 shows sequential activation of the MSF LEDs. The MSF was coated with Loctite EA E-60NC (1:1 resin to hardener mix ratio, Henkel, Germany) for waterproofing. The waterproof coating was left to cure overnight. The sensing sheets were applied as described in the Supporting Information (Figure 4B).

Measurement Parameters. For pH sensing, LED currents were set to 6 mA and HSS-emitted light was sampled at 10Khz. Detection integration times (<1 s) were tuned at the start of each experiment. The tuning occurs in the first test solution of each *in vitro* experiment or following insertion for the *in vivo* experiment. Specifically, integration time was tuned such that the IVC hold voltage ranged between 1 and 2 V, corresponding to 30−61% of the total integration capacity.

For lactate sensing, each of the 625 nm LEDs was illuminated one at a time. The LEDs were driven by a square waveform comprising 21 cycles having a peak current of 9 mA at a frequency of 5 kHz and 25% duty cycle. PtTPTBP emission was sampled simultaneously at 500 kHz. A unique MSF was used for each of the *in vitro* and *in vivo* experiments.

Statistical Analysis. Measurements are reported as the mean and standard error of the mean. Statistical analyses were conducted using a one-way analysis of variance (ANOVA) with Tukey post hoc comparison or coefficient of variance (CV). $p < 0.05$ denotes statistical significance. Prism 8 (GraphPad, USA) was used for statistical analysis.

***In Vivo* Rabbit Study.** The PALS implant study was conducted with the approval of the Institutional Animal Care and Use Committee at the University of California Irvine. A New Zealand white rabbit was sedated with a 2:1 ratio of ketamine hydrochloride (100 mg/mL, Ketaject, Phoenix Pharmaceutical Inc., USA): xylazine (20 mg/mL, Anased, Lloyd Laboratories) at a dose of 37.5 mg/kg of ketamine and 5 mg/kg of xylazine IM using a 25 gauge 5/8 inch needle. The mixture of ketamine and xylazine was infused into the animal's right marginal ear vein. The animal was intubated and placed on mechanical ventilation with a tidal volume of 50 mL per breath, respiratory rate of 20 breaths/min, and 100% oxygen. An arterial catheter was placed within the right femoral artery for systemic blood pressure measurements and arterial blood gas sampling.

The MSF was implanted into the subcutaneous space of the inner left thigh of the rabbit. First, an incision (length = 0.8 cm) was created with a scalpel. Next, Metzenbaum dissecting scissors (Cole-Parmer, USA) were inserted inside the incision to create a pocket by separating the skin from underlying muscle. This pocket runs parallel to the thin skin of the rabbit and accommodates approximately 2 cm of the MSF tip. After MSF-tip insertion, Loctite 4981 adhesive (Henkel, Germany) was applied at the incision site to adhere the MSF onto the skin and seal the incision. The PALS wearable unit was then placed on the skin and aligned to the MSF tip. Hypafix adhesive (USA) was placed over the PALS wearable unit to limit sensor movement. After baseline measurements, the PALS was disconnected, and the animal was placed inside a sealed chamber which was then moved into a fume hood. The animal received 800 ppm chlorine gas (Airgas, USA) for 6 min followed by a 5 min rest period. A total of 1 mL of 100 mM trihistidyl cobinamide was then administered through the right marginal ear vein. The animal was taken back to the surgical room, and the PALS was reconnected to resume monitoring. At the

https://doi.org/10.1021/acssensors.1c01720
ACS Sens. 2022, 7, 441−452

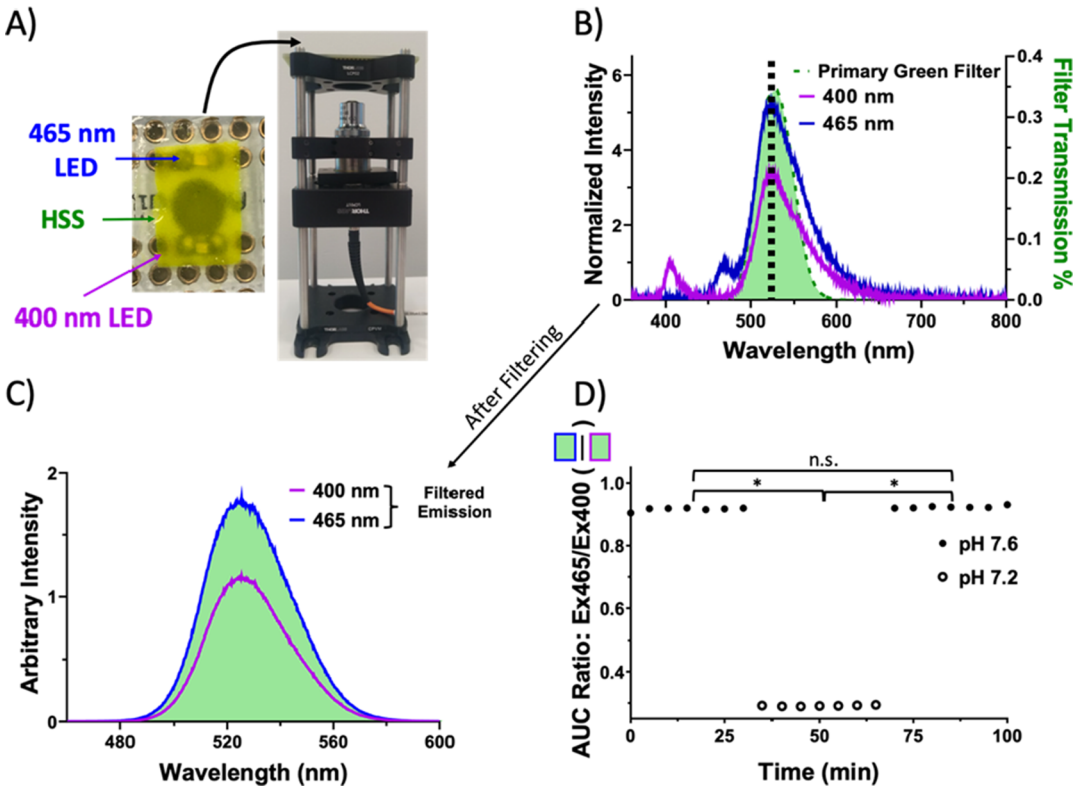

Figure 5. Dual LED excitation of the HSS. (A) (left) 465 nm and 400 nm LEDs soldered onto a protoboard and covered by an HSS; (right) HSS emission signals are collected using a benchtop optical system for analysis. An optical fiber routes the collected light to a spectrometer. (B) Dual emission spectra at pH 7.6. The green spectrum shows the transmission curve of the primary green filter. The black dotted line indicates the HPTS peak emission wavelength. (C) HPTS emission spectra following multiplication with the primary green filter transmission spectrum. (D) AUC ratios for solutions of pH 7.2 and 7.6. Mean ratios were analyzed for statistical significance. *$p < 0.05$.

conclusion of the study, the animal was euthanized as per standard procedures (1 mL of Euthasol, Virbac, USA).

Analysis of *In Vivo* Data. During the study, blood was drawn from the right femoral artery at eight time points. Four blood draws were retrieved before and after chlorine gas and cobinamide infusion. Blood pH and lactate concentration was immediately assessed with an i-STAT (Abbott Laboratories, USA) using Abbott CG4+cartridges (Abbott Laboratories, USA). PALS pH and lactate measurements were retrospectively calibrated to the blood pH and lactate concentrations obtained from the i-STAT with a linear regression model.

RESULTS AND DISCUSSION

pH Sensing by Dual LED Excitation and Single-Band Detection. The PALS uses a dual LED excitation, single-band photodetection scheme for measuring pH. To enable such sensing, the tip of the MSF comprises two surface-mount LEDs to excite an HSS and a coated photodetector to collect pH-sensitive emissions. To first determine if this is a viable scheme, a benchtop optical system was constructed (Figure 5A; fabrication methods in the Supporting Information). This system includes surface-mount 400 nm and 465 nm dominant-wavelength LEDs soldered onto a protoboard and a microscope objective lens that couples emitted light to a spectrometer (Figure 5A). pH-sensitive spectra from an HSS in a pH 7.6 solution were collected with serial illumination from the two LEDs (Figure 5B). The HSS emission spectrum ranges from 470 to 660 nm and has a peak value at 520 nm. While the 400 nm LED light does not overlap the HSS emission spectrum, the 465 nm LED does, necessitating an optical filter that mitigates the effects of this spectral cross talk. Ideally, such a filter should transmit the HSS emission spectrum (Figure 5B) and be easily applied onto the surface of a PD. The primary green filter was selected which can be applied onto a PD as described in the Methods. To simulate the filtering behavior of the primary green filter, its transmission spectrum was multiplied with HSS emission spectra (one per LED). The resulting filtered spectra show that the 465 nm LED light has a negligible contribution to the fluorescence signal (Figure 5C). To test for pH sensitivity and reversibility, HSS spectra in solutions having pH 7.2 or 7.6 were collected and then multiplied by the primary green filter transmission curve. The ratio of area under the curve (AUC Ratio: Ex465/Ex400) was determined at these two pH values. Results indicate that the dual LED, single-band detection scheme is stable and reversible and can be utilized as a pH optode at the tip of the MSF (Figure 5D).

pH Optode. The pH optode comprises three of the optoelectronic elements at the tip of the MSF (Figure 4A). The optode is fabricated by placing an HSS at the tip of the MSF such that it overlaps the two LEDs and filter-coated photodetector (Figure 4B) as described in the Supporting Information. Photocurrents from the photodetector are amplified and converted to a voltage using a transimpedance amplifier. pH is related to the ratio of the voltages acquired with 465 and 400 nm LED illumination ($R_{Ex465/Ex400}$) after background (in the absense of LED emission) subtraction.

Lactate Optode. The lactate optode was adapted from our previous work. In brief, two oxygen-sensitive PtTPTBP dye sheets are mounted on two 625 nm dominant-wavelength LEDs. One of these sheets also contains the enzymes LOX and

https://doi.org/10.1021/acssensors.1c01720
ACS Sens. 2022, 7, 441−452

catalase. The working optode has the enzyme-containing sheet, whereas the reference optode has the enzyme-free sheet. The LEDs are illuminated in sequence, and oxygen-sensitive dye emission is detected using a photodetector within the PALS wearable unit (Figures 1 and 4E).[52] Lactate is related to the phase shift difference between the reference and working optodes. A phase shift (ϕ) is defined as the phase difference (assessed by Fourier transform) between the LED drive-current waveform and the corresponding PD signal at the drive frequency. The Stern−Vollmer equation relates oxygen partial pressure to phosphorescence lifetime under measurement conditions (τ) and in the absence of oxygen (τ_0).[53] ϕ is related to τ by the function $\tan(\phi) = 2\pi f\tau$, where f is the modulation frequency of LED emission.[54] This gives the equations

$$\frac{\tan\phi_0}{\tan\phi_w} = 1 + K_{SV}pO_{2,w} \quad (1)$$

$$\frac{\tan\phi_0}{\tan\phi_R} = 1 + K_{SV}pO_{2,R} \quad (2)$$

where ϕ_w and ϕ_R correspond to the working and reference optode, respectively, ϕ_0 corresponds to the absence of oxygen, K_{sv} is the Stern Vollmer constant, and $pO_{2,w}$ and $pO_{2,R}$ are the oxygen partial pressures at the working and reference optode, respectively.

Subtracting eq 1 from eq 2 yields

$$\frac{\tan\phi_0}{\tan\phi_R} - \frac{\tan\phi_0}{\tan\phi_w} = 1 + K_{SV}pO_{2,R} - (1 + K_{SV}pO_{2,w}) \quad (3)$$

which can be rewritten to define the sensor signal β

$$\beta = \frac{\tan\phi_w - \tan\phi_R}{\tan\phi_w\tan\phi_R} = \frac{K_{SV}}{\tan\phi_0}(pO_{2,R} - pO_{2,w}) \quad (4)$$

Here, $\frac{K_{SV}}{\tan\phi_0}$ is a proportionality constant determined through linear calibration in a series of lactate solutions at room air.

pH Sensing *In Vitro*. To determine baseline pH sensor stability, measurements were obtained every 30 min for 8 h in pH 7.45 solution. Unless otherwise stated, each reported steady-state measurement is an average of 20 single-point measurements acquired in succession. No signal drift was detected (Figure S4; CV = 0.002). The stability is due in part to the quality of our custom LED current control circuitry (provided by the TLC driver, Figure S2A) that produces consistent LED output power. To check the stability of both LEDs, their emission spectra were acquired every 3 min for 30 min. Spectra show no significant differences in AUC (CV = 0.001) or peak emission intensity (CV ≤ 0.002; Figure S5). pH sensing rise time was assessed by first incubating a sensor in a solution with pH 7.45 and then exchanging for a solution with pH 7.01. $R_{Ex400/Ex465}$ (the ratio of detector signals under 400nm and 465 nm excitation) was measured every 4.8 s following media exchange. Response kinetics are described using a rising exponential plateau model (R^2 = 0.99, standard error of the estimate ($Sy.x$) = 0.006) with a t90 rise time of 2.01 min (Figure 6A). This rise time is short enough to capture critical physiological events such as subdermal scalp acidosis following fetal tachycardia in high-risk births, which occur on the time scale of minutes.[55]

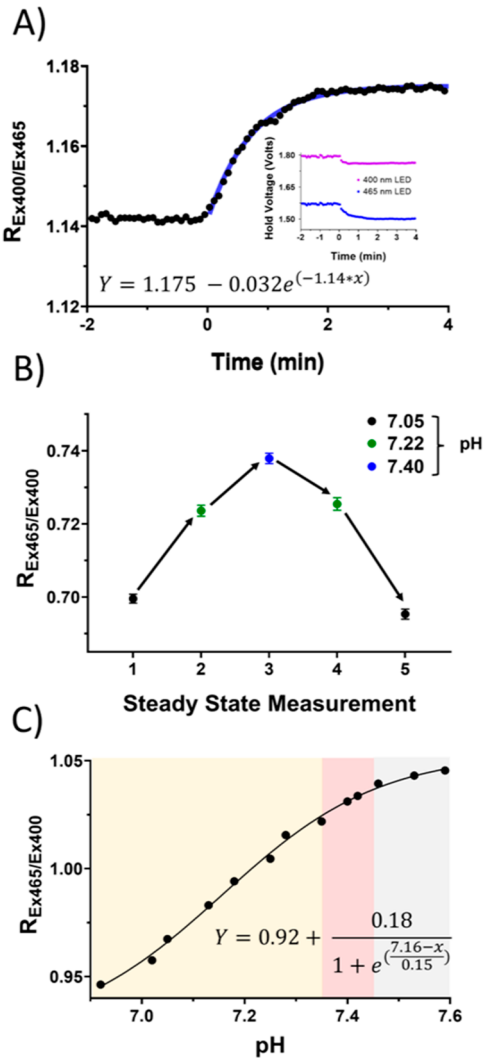

Figure 6. Ratiometric pH Sensing. (A) pH sensor rise time from pH 7.45 to 7.01. The inset shows the hold voltages for each LED. (B) pH sensor steady-state measurements in a series of pH solutions. Arrows indicate the sequence of test solutions. (C) Calibration curve. The red shaded region indicates a normal physiological range of pH in blood, 7.35−7.45, while the orange and gray shaded regions indicate acidosis and alkalosis, respectively.

pH sensing reversibility was assessed by sequential measurements of solutions having a pH of 7.05, 7.22, 7.40, 7.22, and 7.05, in that order (Figure 6B). To obtain a steady measurement at each pH, the sensor was first washed ten times with that pH solution. One-way ANOVA indicates a significant effect across groups ($p \ll 0.01$). Tukey post hoc comparison with adjusted p-values shows significant differences between the three unique pH solutions ($p \ll 0.01$ for each comparison) but no significant differences between repeated pH solutions ($p > 0.25$ for each comparison). pH sensing sensitivity and range were assessed by exposure to 13 solutions, with pH ranging from 6.92 to 7.59. Data follow a Boltzmann sigmoidal model ($R^2 > 0.99$ and $Sy.x = 0.002$) with a pK_a of 7.16 (Figure 6C), which is similar to the pK_a of the HPTS dye alone.[25] Importantly, wellness-of-fit indicates that PALS will have clinical relevance across the pathophysiological range including acidosis and alkalosis.[56]

Lactate Sensing *In Vitro*. To determine lactate sensor stability, measurements were obtained every 30 min for 4 h in

https://doi.org/10.1021/acssensors.1c01720
ACS Sens. 2022, 7, 441−452

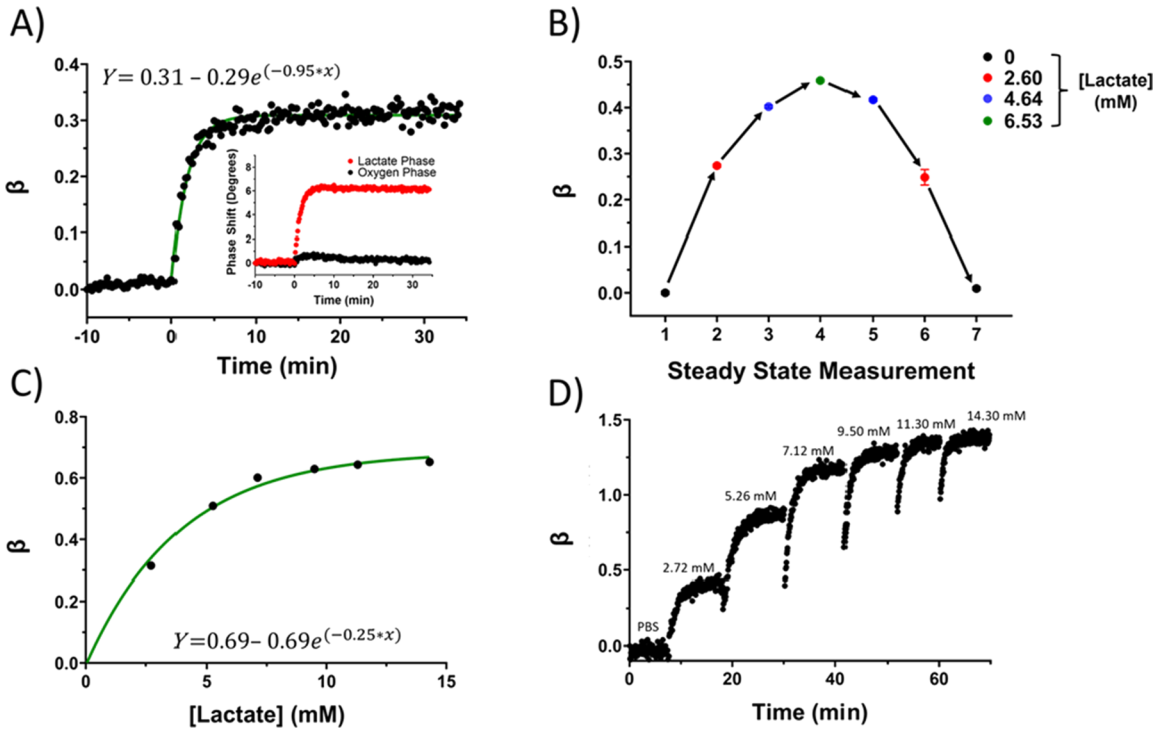

Figure 7. *In vitro* lactate sensing. (A) Rise time measured after media exchange from 0 to 6 mM lactate. The inset represents the raw lactate and oxygen phase shift measurements. (B) β for a series of test solutions. (C) Lactate sensor calibration and (D) β acquired during the calibration experiment. Green lines in A and C represent model fit to the data (equation is listed next to each curve).

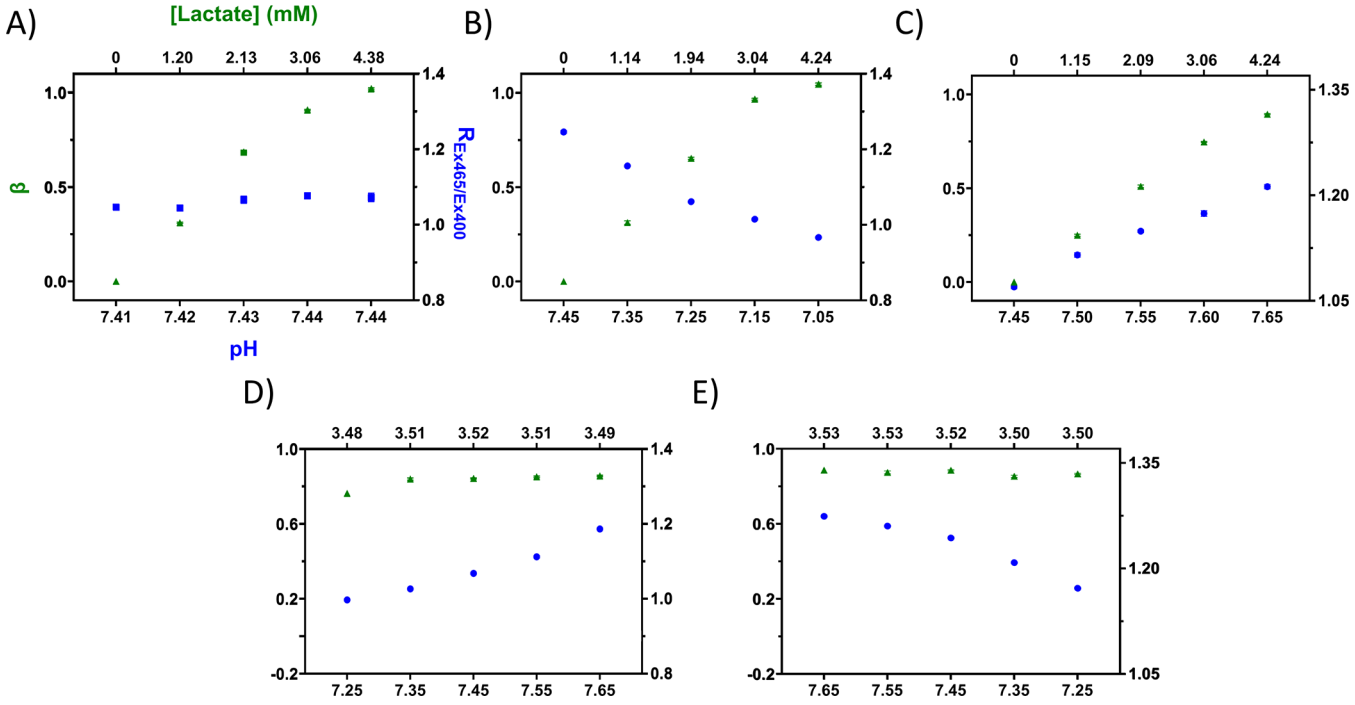

Figure 8. pH and lactate multianalyte sensing. A series of solutions were formulated to model pathological conditions. Solutions were formulated then measured with a Mettler Toledo FiveEasy pH probe and YSI 2300 STAT Plus Glucose and Lactate Analyzer; values are shown on the horizontal axes. Solutions were tested by PALS in order from left to right. Solutions model: (A) hyperlactatemia, (B) lactic acidosis, (C) respiratory alkalosis and hyperlactatemia, (D) extreme metabolic alkalosis, and (E) respiratory acidosis.

4 mM lactate solution. Unless otherwise stated, each reported steady-state value is the mean of 10 measurements. No significant signal drift was detected (Figure S6; CV = 0.007). The stability is due in part to the inclusion of the enzyme catalase that scavenges hydrogen peroxide, known to degrade proteins.[57,58] In this reaction, iron in catalase extracts one oxygen molecule from hydrogen peroxide, producing a single water molecule. Then, another oxygen molecule from a second hydrogen peroxide molecule binds to the oxygen-bound catalase, producing a second water molecule. Molecular oxygen

https://doi.org/10.1021/acssensors.1c01720
ACS Sens. 2022, 7, 441−452

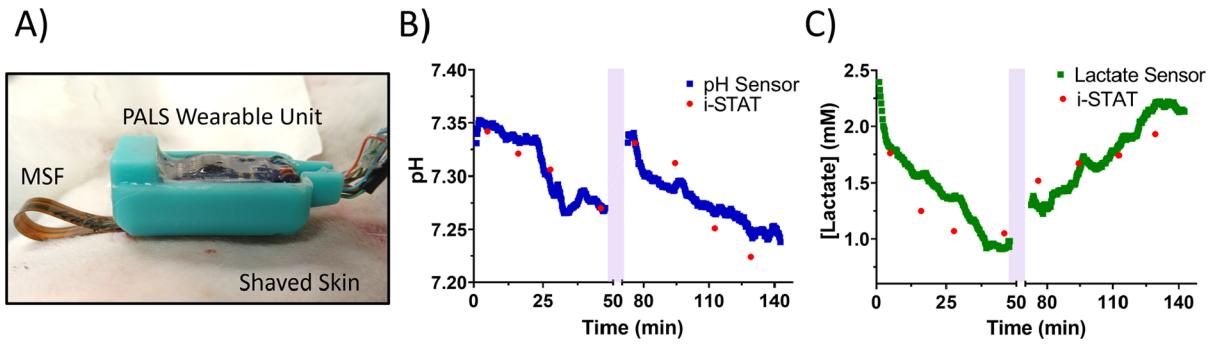

Figure 9. *In vivo* multianalyte sensing in a rabbit exposed to chlorine gas. The purple region indicates when PALS measurements were paused for chlorine gas and cobinamide administration. (A) Sensor implanted in the subcutaneous space of the inner left thigh. Lactate (B) and pH (C) sensing signals with intermittent blood reference values (i-STAT).

is then released from the catalase.[59] Lactate sensing rise time was then assessed by changing the test media from 0 mM (1× phosphate-buffered saline solution, PBS) to 6 mM lactate. Phase shifts were recorded and β was calculated every 12 s following media exchange. Response kinetics follow an exponential plateau model (R^2 = 0.95 and *Sy.x* = 0.01) with a t90 rise time of 3.65 min (Figure 7A). This rise time is comparable to commercial continuous glucose monitors such as the Dexcom G6 and Medtronic Guardian, which are reported to have an average rise time *in vivo* of 9.5 min and are effective in guiding insulin therapy.[60]

Lactate sensing reversibility was evaluated by sequential testing of lactate solutions having concentrations of 0, 2.60, 4.64, 6.53, 4.64, 2.60, and 0 mM (Figure 7B). To obtain a steady measurement at each lactate concentration, the sensor was first washed ten times with that lactate solution, after which measurements were obtained. One-way ANOVA detected differences between groups ($p \ll 0.01$). Tukey post hoc comparison with adjusted *p*-values shows no significant differences between the pairing of identical lactate solutions ($p > 0.87$), while significant differences were found between solutions of different lactate concentrations ($p \ll 0.01$). Lactate sensitivity and range were evaluated by incubation in seven lactate solutions ranging in concentration from 0 to 14 mM. Data follow an exponential plateau model (R^2 = 0.99 and *Sy.x* = 0.03), showing sensitivity to lactate from 0 to 9 mM (Figure 7C). Discrete β measurements are shown in Figure 7D. These results show that PALS lactate sensing can distinguish between concentrations within the pathophysiological range.

Multianalyte Sensing *In Vitro*. Combined pH and lactate sensing was tested using *in vitro* models of five pathophysiological conditions (Figure 8). The conditions were designed to capture sensitivity and trends of both pH and lactate in such pathologies and to detect any interference or cross talk. A series of test solutions with prescribed pH and lactate concentration were formulated and analyzed using calibrated instruments (a Mettler Toledo FiveEasy pH probe and a YSI 2300 STAT Plus Glucose and Lactate Analyzer). Solutions were then probed using PALS in an order corresponding to each model. In a model of hyperlactatemia, pH was maintained at 7.43 ± 0.02 while lactate was increased (Figure 8A). PALS signals report the increase in lactate, while the pH signals did not significantly change (CV = 0.018). In a model of lactic acidosis, as experienced in sepsis, solutions were formulated to have a decrease in pH and an increase in lactate (Figure 8B), and PALS successfully reports these changes. In a model of panic-disorder patients who exhibit both respiratory alkalosis and hyperlactatemia, solutions were formulated to have an increase in both pH and lactate concentrations.[3] PALS signals successfully reflect these increases (Figure 8C). In a model of extreme metabolic alkalosis, as can occur with chronic vomiting and diarrhea, pH was increased while lactate was held at 3.50 mM ± 0.02 (Figure 8D).[61] PALS signals report the increase in pH and constant lactate concentration (CV = 0.037). In a model of respiratory acidosis (as seen in chronic obstructive pulmonary disease), pH was formulated to decrease while lactate levels were held constant at 3.52 ± 0.02 (Figure 8E).[62] PALS signals report the decrease in pH and constant lactate concentrations (CV = 0.016).

To test for and quantify signal interference, correlation between lactate concentration and pH (as measured by analytical instruments) in test solutions was first determined by aggregating values across all experiments (Figure 8A–E). The Pearson's product-moment coefficient was low (−0.01) with a nonsignificant *p*-value (0.95), confirming independence within test solutions. Next, to test for correlations between the two sensing modalities, we aggregated raw signals across all experiments. The Pearson's product-moment coefficient was low (−0.1) with a nonsignificant *p*-value (0.68). This insignificant correlation demonstrates the lack of interference between PALS sensing modalities.

Collectively, Figure 8 demonstrates that PALS does not exhibit sensing modality cross talk and can report physiologically relevant pH and lactate changes, which may aid clinicians in their practice of analyte-guided treatment toward improving patient outcome.

Multianalyte Sensing *In Vivo*. PALS multianalyte sensing was tested in an *in vivo* rabbit model of chlorine gas poisoning and cobinamide treatment. When chlorine gas reacts with water in the lungs, hydrochloric and hypochlorous acid are produced. The production of these acids damages the respiratory mucus membrane resulting in pulmonary edema and hypoxemia.[61,63] PALS should therefore detect decreasing pH and increasing lactate values following chlorine gas administration. At the start of the experiment, the MSF tip was implanted and connected to the wearable unit (Figure 9A) for data collection (LED serial illumination shown in Video S2). PALS signals were converted to analyte values using retrospective linear regression (Figure S7). Both blood pH and lactate concentration decreased prior to drug infusion as measured by PALS and intermittent i-STAT blood assays (Figure 9B,C). These decreases may be a function of the sedative chemistry and the ventilation control. After poisoning

https://doi.org/10.1021/acssensors.1c01720
ACS Sens. 2022, 7, 441−452

and cobinamide treatment, PALS detected the expected increase in lactate concentration and decrease in blood pH, which were also in agreement with the intermittent i-STAT blood assays (Figure 9B,C). The area under the concentration-time curve ratio between PALS and i-STAT measurements was calculated and assessed as described in Dror et al., following FDA guidelines.[39,64] The area under the concentration-time curve ratio for pH (0.979) and lactate (1.084) indicates PALS bioequivalence to the i-STAT blood analyzer in this study. There is a difference in pH measurements between i-STAT and PALS beginning at 110 min. PALS reports a higher pH value, with a difference of approximately 0.025. In previous work, Bland-Altman analysis comparing i-STAT to i-Smart and pHO*x* ultra-pH meters shows that i-Stat underestimates pH (relatively) by as much as 0.5 for values of pH < 7.3, indicating that the i-STAT may be a source of error for the last two time points of blood comparisons.[65] Results demonstrate that PALS reports clinically relevant pH and lactate changes and at a higher frequency than can be offered by blood analysis alone.

CONCLUSIONS

We have shown that two different photonic detection schemes on an implanted flexible sensor can yield reliable signals for monitoring both pH and lactate across clinically relevant ranges. Our results suggest that PALS can be used as a one-day device, which in many cases is sufficient in the ICU considering the ease of replacement and the average ICU stay. As pH and lactate values are strong predictors of mortality, the ability to provide stable and reliable measurements of pH and lactate, on the time scale of minutes to hours, can be utilized to guide therapy and improve patient outcome.[15,66] However, the technology should be improved before it can be used in the clinic over extended periods. Because the process of PALS fabrication is not controlled at the level expected for a commercial product, we do observe differences in calibration parameters between units. Currently, methods are being developed by our group to reduce variances in sheet fabrication and to improve the process by which the plastic optical filter is applied onto the photodetector. Additional engineering development will include miniaturization of the backend electronics to include a battery as well as wireless data control and acquisition, which are achievable by the existing manufacturing methods. In regard to miniaturizing the MSF, our research group has successfully reduced the lactate optode to a width of 300 μm.[39] For the pH optode, the dimensions of the photodetector are the limiting factor for miniaturization. In future work, we will incorporate photodetectors having dimensions similar to the MSF LEDs, yielding a 1/3 mm wide device.

PALS can have a major impact on patient outcomes under conditions such as sepsis and organ failure where attentive monitoring of pH and lactate has been reported to improve patient outcome.[1−4] Importantly, the core elements of PALS can be replicated and modified to sense additional analytes on the MSF. For example, similar to the operating principle of HPTS, fluorescent dyes Fura Red AM and SBFI-AM exhibit a change in their absorbance behavior based on the concentration of calcium and sodium, respectively.[67,68] Consequently, our dual-excitation, single-band detection scheme could be readily employed to continuously monitor these analytes. Moreover, our lactate sensing scheme is generalizable to additional oxidases and their corresponding analytes including glucose and alcohol.[69,70] The addition of these analytes can broaden the applicability of the MSF to other medical conditions. For example, continuous monitoring of sodium, pH, lactate, oxygen, and glucose in individuals experiencing diabetic ketoacidosis can diagnose dehydration (loss of sodium), ketoacidosis (high glucose and low pH), and ischemia (low oxygen and high lactate), directing healthcare professionals toward a specific mode of intervention.[71−73] An expanded MSF could also be applicable beyond the medical field, such as in bioreactors for protein expression, agriculture, water management, and food industry, where sensing pH, glucose, and sodium would provide vital information to each respective field.[74−77]

ASSOCIATED CONTENT

Supporting Information

The Supporting Information is available free of charge at https://pubs.acs.org/doi/10.1021/acssensors.1c01720.

Additional material that supports the findings of the study, information regarding construction of the spectroscopic benchtop system, formulating the pH and lactate test solutions, main PALS circuit components and connections, image of the filter-coated photodetector, raw LED spectra, LED stability studies, and both baseline lactate and pH sensing stability data sets (PDF)

Serial MSF LED activation *in vitro* (MP4)

Serial MSF LED activation *in vivo* (MP4)

AUTHOR INFORMATION

Corresponding Author

Elliot L. Botvinick − *Department of Biomedical Engineering, University of California Irvine, Irvine, California 92697-2730, United States; Beckman Laser Institute and Medical Clinic, University of California Irvine, Irvine, California 92612, United States; Edwards Lifesciences Foundation Cardiovascular Innovation and Research Center, University of California Irvine, Irvine, California 92697, United States; Department of Surgery, University of California, Irvine, California 92697-2730, United States;* orcid.org/0000-0001-9837-805X; Email: elliot.botvinick@uci.edu

Authors

Dat Nguyen − *Department of Biomedical Engineering, University of California Irvine, Irvine, California 92697-2730, United States; Beckman Laser Institute and Medical Clinic, University of California Irvine, Irvine, California 92612, United States; Edwards Lifesciences Foundation Cardiovascular Innovation and Research Center, University of California Irvine, Irvine, California 92697, United States;* orcid.org/0000-0001-5582-7222

Micah M. Lawrence − *Department of Biomedical Engineering, University of California Irvine, Irvine, California 92697-2730, United States; Beckman Laser Institute and Medical Clinic, University of California Irvine, Irvine, California 92612, United States; Edwards Lifesciences Foundation Cardiovascular Innovation and Research Center, University of California Irvine, Irvine, California 92697, United States*

Haley Berg − *Edwards Lifesciences Foundation Cardiovascular Innovation and Research Center, University of California Irvine, Irvine, California 92697, United States*

Monika Aya Lyons − *Department of Biomedical Engineering, University of California Irvine, Irvine, California 92697-*

2730, United States; Beckman Laser Institute and Medical Clinic, University of California Irvine, Irvine, California 92612, United States; Edwards Lifesciences Foundation Cardiovascular Innovation and Research Center, University of California Irvine, Irvine, California 92697, United States

Samir Shreim − *Beckman Laser Institute and Medical Clinic, University of California Irvine, Irvine, California 92612, United States*

Mark T. Keating − *Beckman Laser Institute and Medical Clinic, University of California Irvine, Irvine, California 92612, United States*

John Weidling − *Beckman Laser Institute and Medical Clinic, University of California Irvine, Irvine, California 92612, United States*

Complete contact information is available at: https://pubs.acs.org/10.1021/acssensors.1c01720

Author Contributions

The manuscript was written through contributions of all authors. All authors have given approval to the final version of the manuscript.

Notes

The authors declare no competing financial interest.

■ ACKNOWLEDGMENTS

This work was supported by the National Institute of Environmental Health Sciences (award number—U54NSES027698), the National Heart, Lung, and Blood Institute (award number—T32HL116270), and the National Institute of General Medical Sciences (award number—T34GM069337). The content is solely the responsibility of the authors and does not necessarily represent the official views of the National Institutes of Health. Research in this publication was also supported by the JDRF (2-SRA-2017-330-Q-R) and the Leona M. and Harry B. Helmsley Charitable Trust (2018PG-T1D008). We would like to thank the laboratory of Dr. Mathew Brenner at UC Irvine for conducting the animal study. We would like to thank the University of California, San Diego, for trihistidyl cobinamide.

■ ABBREVIATIONS

PtTPTBP, dye platinum(II) meso-tetraphenyl tetrabenzoporphine; HPTS, 8-hydroxypyrene-1,3,6-trisulfonic acid trisodium salt; LOX, lactate oxidase; PALS, pH and lactate sensor; H^+, hydrogen ion; HSS, pH sensor sheet; MSF, multisensing flexible sensor; PBS, phosphate-buffered saline solution; PTFE, polytetrafluoroethylene; UV, ultraviolet; CV, coefficient of variance; *Sy.x*, standard error of the estimate; R^2, coefficient of determination; LED, light-emitting diode; ANOVA, one-way analysis of variance; AUC, area under the curve; YSI, Yellow Springs Instrument; Irgacure 2959, 2-hydroxy-1-(4-(2-hydroxyethoxy)phenyl)-2-methylpropan-1-one; ppm, parts per million; $R_{Ex465/Ex400}$, voltage ratio after 465 and 400 nm LED excitation; PEGDMA, poly(ethylene glycol) dimethacrylate; PEGDA, poly(ethylene glycol) diacrylate; AUC Ratio Ex465/Ex400, spectra ratio after 465 and 400 nm LED excitation

■ REFERENCES

(1) Lee, S.-W.; Hong, Y.-S.; Park, D.-W.; Choi, S.-H.; Moon, S.-W.; Park, J.-S.; Kim, J.-Y.; Baek, K.-J. Lactic Acidosis Not Hyperlactatemia as a Predictor of Inhospital Mortality in Septic Emergency Patients. *Emerg. Med. J.* **2008**, *25*, 659−665.

(2) Scheiner, B.; Lindner, G.; Reiberger, T.; Schneeweiss, B.; Trauner, M.; Zauner, C.; Funk, G.-C. Acid-Base Disorders in Liver Disease. *J. Hepatol.* **2017**, *67*, 1062−1073.

(3) Hall, A. M.; Bending, M. R. Severe Hyperlactaemia in the Setting of Alkalaemia. *NDT Plus* **2009**, *2*, 408−411.

(4) Kellum, J. A. Determinants of Blood PH in Health and Disease. *Crit. Care* **2000**, *4*, 6−14.

(5) Awati, M. N.; Mudda, V.; Chandra, M.; Samudyatha, T. J. Of Acid Base Balance. *J. Evidence-Based Med. Healthc.* **2014**, *1*, 2140.

(6) Zilva, J. F. The Origin of the Acidosis in Hyperlactataemia. *Ann. Clin. Biochem.* **1978**, *15*, 40−43.

(7) Foucher, C. D.; Tubben, R. E. *Lactic Acidosis*; StatPearls, 2020.

(8) Meakins, J.; Long, C. N. H. Oxygen Consumption, Oxygen Debt And Lactic Acid In Circulatory Failure 1. *J. Clin. Invest.* **1927**, *4*, 273−293.

(9) Patel, S.; Sharma, S. *Respiratory Acidosis*; StatPearls 2021.

(10) Dukić, L.; Kopčinović, L. M.; Dorotić, A.; Baršić, I. Blood Gas Testing and Related Measurements: National Recommendations on Behalf of the Croatian Society of Medical Biochemistry and Laboratory Medicine. *Biochem. Med.* **2016**, *26*, 318−336.

(11) White, R.; Yaeger, D.; Stavrianeas, S. Determination of Blood Lactate Concentration: Reliability and Validity of a Lactate Oxidase-Based Method. *Int. J. Exerc. Sci.* **2009**, *2*, 2.

(12) Steinfelder-Visscher, J.; Teerenstra, S.; Gunnewiek, J. M.; Weerwind, P. W. Evaluation of the I-STAT Point-of-Care Analyzer in Critically Ill Adult Patients. *J. Extra Corpor. Technol.* **2008**, *40*, 57.

(13) Bodley, T.; Chan, M.; Clarfield, L.; Levi, O.; Longmore, A.; Lin, W.; Yip, D.; Orla, S.; Friedrich, J. O.; Hicks, L. K. Patient Harm from Repetitive Blood Draws and Blood Waste in the ICU: A Retrospective Cohort Study. *Blood* **2019**, *134*, 57.

(14) Pölönen, P.; Ruokonen, E.; Hippeläinen, M.; Pöyhönen, M.; Takala, J. A Prospective, Randomized Study of Goal-Oriented Hemodynamic Therapy in Cardiac Surgical Patients. *Anesth. Analg.* **2000**, *90*, 1052−1059.

(15) Friedman, G.; et al. Combined measurements of blood lactate concentrations and gastric intramucosal pH in patients with severe sepsis. *Crit. Care Med.* **1995**, *23*, 1184.

(16) Jansen, T. C.; van Bommel, J.; Mulder, P. G.; Rommes, J. H.; Schieveld, S. J. M.; Bakker, J. The Prognostic Value of Blood Lactate Levels Relative to That of Vital Signs in the Pre-Hospital Setting: A Pilot Study. *Crit. Care* **2008**, *12*, R160.

(17) Ganesh, K.; Sharma, R.; Varghese, J.; Pillai, M. G. K. A Profile of Metabolic Acidosis in Patients with Sepsis in an Intensive Care Unit Setting. *Int. J. Crit. Illness Inj. Sci.* **2016**, *6*, 178.

(18) Manjakkal, L.; Szwagierczak, D.; Dahiya, R. Metal Oxides Based Electrochemical PH Sensors: Current Progress and Future Perspectives. *Prog. Mater. Sci.* **2020**, *109*, 100635.

(19) Vonau, W.; Guth, U. PH Monitoring: A Review. *J. Solid State Electrochem.* **2006**, *10*, 746−752.

(20) Khan, M. I.; Mukherjee, K.; Shoukat, R.; Dong, H. A Review on PH Sensitive Materials for Sensors and Detection Methods. *Microsyst. Technol.* **2017**, *23*, 4391−4404.

(21) Miksa, M.; Komura, H.; Wu, R.; Shah, K. G.; Wang, P. A Novel Method to Determine the Engulfment of Apoptotic Cells by Macrophages Using PHrodo Succinimidyl Ester. *J. Immunol. Methods* **2009**, *342*, 71−77.

(22) Boens, N.; Qin, W.; Basarić, N.; Orte, A.; Talavera, E. M.; Alvarez-Pez, J. M. Photophysics of the Fluorescent PH Indicator BCECF. *J. Phys. Chem. A* **2006**, *110*, 9334−9343.

(23) Ramshesh, V. K.; Lemasters, J. J. Imaging of Mitochondrial PH Using SNARF-1. *Methods Mol. Biol.* **2012**, *810*, 243−248.

(24) Jokic, T.; Borisov, S. M.; Saf, R.; Nielsen, D. A.; Kühl, M.; Klimant, I. Highly Photostable Near-Infrared Fluorescent PH Indicators and Sensors Based on BF2-Chelated Tetraarylazadipyrromethene Dyes. *Anal. Chem.* **2012**, *84*, 6723−6730.

(25) Kermis, H. R.; Kostov, Y.; Harms, P.; Rao, G. Dual Excitation Ratiometric Fluorescent PH Sensor for Noninvasive Bioprocess

Monitoring: Development and Application. *Biotechnol. Prog.* **2002**, *18*, 1047−1053.
(26) An, Y.; Bai, H.; Li, C.; Shi, G. Disassembly-Driven Colorimetric and Fluorescent Sensor for Anionic Surfactants in Water Based on a Conjugated Polyelectrolyte/Dye Complex. *Soft Matter* **2011**, *7*, 6873−6877.
(27) Hulth, S.; Aller, R. C.; Engström, P.; Selander, E. A PH Plate Fluorosensor (Optode) for Early Diagenetic Studies of Marine Sediments. *Limnol. Oceanogr.* **2002**, *47*, 212−220.
(28) Hakonen, A.; Hulth, S. A High-Precision Ratiometric Fluorosensor for PH: Implementing Time-Dependent Non-Linear Calibration Protocols for Drift Compensation. *Anal. Chim. Acta* **2008**, *606*, 63−71.
(29) Wencel, D.; Kaworek, A.; Abel, T.; Efremov, V.; Bradford, A.; Carthy, D.; Coady, G.; McMorrow, R. C. N.; McDonagh, C. Optical Sensor for Real-Time PH Monitoring in Human Tissue. *Small* **2018**, *14*, 1803627.
(30) Yanase, S.; Yasuda, K.; Ishii, N. Small-Scale Colorimetric Assays of Intracellular Lactate and Pyruvate in the Nematode Caenorhabditis Elegans. *J. Visualized Exp.* **2018**, *140*, No. e57807.
(31) Erdoğan, H.; Ünübol Aypak, S.; Erdoğan, S.; Ural, K. Comparative Interpretation of Lactate Measurement by Point of Care Spectrophotometric and ELISA Methodsin Transition Cows. *Pol. J. Vet. Sci.* **2018**, *21*, 741−746.
(32) Rathee, K.; Dhull, V.; Dhull, R.; Singh, S. Biosensors Based on Electrochemical Lactate Detection: A Comprehensive Review. *Biochem. Biophys. Rep.* **2016**, *5*, 35−54.
(33) Park, J.; Sempionatto, J. R.; Kim, J.; Jeong, Y.; Gu, J.; Wang, J.; Park, I. Microscale Biosensor Array Based on Flexible Polymeric Platform toward Lab-on-a-Needle: Real-Time Multiparameter Biomedical Assays on Curved Needle Surfaces. *ACS Sens.* **2020**, *5*, 1363−1373.
(34) Payne, M. E.; Zamarayeva, A.; Pister, V. I.; Yamamoto, N. A. D.; Arias, A. C. Printed, Flexible Lactate Sensors: Design Considerations Before Performing On-Body Measurements. *Sci. Rep.* **2019**, *9*, 13720.
(35) Currano, L. J.; Sage, F. C.; Hagedon, M.; Hamilton, L.; Patrone, J.; Gerasopoulos, K. Wearable Sensor System for Detection of Lactate in Sweat. *Sci. Rep.* **2018**, *8*, 15890.
(36) Maahs, D. M.; Desalvo, D.; Pyle, L.; Ly, T.; Messer, L.; Clinton, P.; Westfall, E.; Wadwa, R. P.; Buckingham, B. Effect of Acetaminophen on CGM Glucose in an Outpatient Setting. *Diabetes Care* **2015**, *38*, e158−e159.
(37) Juska, V. B.; Pemble, M. E. A Critical Review of Electrochemical Glucose Sensing: Evolution of Biosensor Platforms Based on Advanced Nanosystems. *Sensors* **2020**, *20*, 6013.
(38) Andrus, L.; Unruh, R.; Wisniewski, N.; McShane, M. Characterization of Lactate Sensors Based on Lactate Oxidase and Palladium Benzoporphyrin Immobilized in Hydrogels. *Biosensors* **2015**, *5*, 398.
(39) Dror, N.; Weidling, J.; White, S.; Ortenzio, F.; Shreim, S.; Keating, M. T.; Pham, H.; Radom-Aizik, S.; Botvinick, E. Clinical Evaluation of a Novel Subcutaneous Lactate Monitor. *J. Clin. Monit. Comput.* **2021**, *2021*, 1−7.
(40) Valledor, M.; Campo, J. C.; Sánchez-Barragán, I.; Costa-Fernández, J. M.; Alvarez, J. C.; Sanz-Medel, A. Determination of Phosphorescence Lifetimes in the Presence of High Background Signals Using Phase-Shift Measurements. *Sens. Actuators, B* **2006**, *113*, 249−258.
(41) Spencer, K. C.; Sy, J. C.; Ramadi, K. B.; Graybiel, A. M.; Langer, R.; Cima, M. J. Characterization of Mechanically Matched Hydrogel Coatings to Improve the Biocompatibility of Neural Implants. *Sci. Rep.* **2017**, *7*, 1952.
(42) Rahoui, N.; Jiang, B.; Taloub, N.; Huang, Y. D. Spatio-Temporal Control Strategy of Drug Delivery Systems Based Nano Structures. *J. Controlled Release* **2017**, *255*, 176−201.
(43) Fourniols, T.; Randolph, L. D.; Staub, A.; Vanvarenberg, K.; Leprince, J. G.; Préat, V.; des Rieux, A.; Danhier, F. Temozolomide-Loaded Photopolymerizable PEG-DMA-Based Hydrogel for the Treatment of Glioblastoma. *J. Controlled Release* **2015**, *210*, 95−104.
(44) Roina, Y.; Auber, F.; Hocquet, D.; Herlem, G. EPTFE Functionalization for Medical Applications. *Mater. Today Chem.* **2021**, *20*, 100412.
(45) Jaganathan, S. K.; Supriyanto, E.; Murugesan, S.; Balaji, A.; Asokan, M. K. Biomaterials in Cardiovascular Research: Applications and Clinical Implications. *BioMed Res. Int.* **2014**, *2014*, 459465.
(46) Mikhailov, I. v.; Sidorchuk, S. v.; Lavrusenko, S. R. Polytetrafluoroethylene in Medicine. *Plast. Massy* **2002**, *29*, 49−52.
(47) FDA Guidance: Device Biocompatibility|Intact Skin|NAMSA. https://namsa.com/fda-releases-new-draft-guidance-for-biocompatibility-of-devices-in-contact-with-intact-skin/(accessed Oct 15, 2021).
(48) Patel, P. J.; Benasi, K.; Ferrari, G.; Evans, M. G.; Shanmugham, S.; Wilson, D. M.; Buckingham, B. A. Randomized Trial of Infusion Set Function: Steel versus Teflon. *Diabetes Technol. Ther.* **2014**, *16*, 15−19.
(49) Lin, C.-C.; Anseth, K. S. PEG Hydrogels for the Controlled Release of Biomolecules in Regenerative Medicine. *Pharm. Res.* **2008**, *26*, 631−643.
(50) Richardson, R. R.; Miller, J. A.; Reichert, W. M. Polyimides as Biomaterials: Preliminary Biocompatibility Testing. *Biomaterials* **1993**, *14*, 627−635.
(51) Constantin, C. P.; Aflori, M.; Damian, R. F.; Rusu, R. D. Biocompatibility of Polyimides: A Mini-Review. *Materials* **2019**, *12*, 3166.
(52) Smith, A. M.; Mancini, M. C.; Nie, S. Bioimaging: Second Window for in Vivo Imaging. *Nat. Nanotechnol.* **2009**, *4*, 710−711.
(53) Tengberg, A.; Hovdenes, J.; Andersson, H. J.; Brocandel, O.; Diaz, R.; Hebert, D.; Arnerich, T.; Huber, C.; Körtzinger, A.; Khripounoff, A.; Rey, F.; Rönning, C.; Schimanski, J.; Sommer, S.; Stangelmayer, A. Evaluation of a Lifetime-Based Optode to Measure Oxygen in Aquatic Systems. *Limnol. Oceanogr.: Methods* **2006**, *4*, 7−17.
(54) Pasic, A.; Koehler, H.; Klimant, I.; Schaupp, L. Miniaturized Fiber-Optic Hybrid Sensor for Continuous Glucose Monitoring in Subcutaneous Tissue. *Sens. Actuators, B* **2007**, *122*, 60−68.
(55) Young, B. K.; Hirschl, I. T.; Klein, S. H.; Katz, M. 25. Continuous Fetal Tissue PH Monitoring in Labor with High Risk Pregnancies. *Arch. Gynecol.* **1978**, *226*, 169.
(56) Hopkins, E.; Sanvictores, T.; Sharma, S. Physiology, Acid Base Balance; StatPearls, 2021; pp 19−22.
(57) Fligiel, S. E.; Lee, E. C.; Mccoy, J. P.; Johnson, K. J.; Varani, J. Protein Degradation Following Treatment with Hydrogen Peroxide. *Am. J. Pathol.* **1984**, *115*, 418.
(58) Davies, M. J. Protein Oxidation and Peroxidation. *Biochem. J.* **2016**, *473*, 805−825.
(59) Trawczyńska, I. New Method of Determining Kinetic Parameters for Decomposition of Hydrogen Peroxide by Catalase. *Catalysts* **2020**, *10*, 323.
(60) Schmelzeisen-Redeker, G.; Schoemaker, M.; Kirchsteiger, H.; Freckmann, G.; Heinemann, L.; del Re, L. Time Delay of CGM Sensors: Relevance, Causes, and Countermeasures. *J Diabetes Sci Technol.* **2015**, *9*, 1006−1015.
(61) Ueda, Y.; Aizawa, M.; Takahashi, A.; Fujii, M.; Isaka, Y. Exaggerated Compensatory Response to Acute Respiratory Alkalosis in Panic Disorder Is Induced by Increased Lactic Acid Production. *Nephrol., Dial., Transplant.* **2009**, *24*, 825−828.
(62) Pahal, P.; Sharma, S. *Chronic Obstructive Pulmonary Disease (COPD) Compensatory Measure*; StatPearls Publishing, 2019.
(63) Gorguner, M.; Akgun, M. Acute Inhalation Injury. *Eurasian J. Med.* **2010**, *42*, 28−35.
(64) Office of Training and Communications Division of Communications Management Drug Information Branch. 2001; pp 301−827.
(65) Cho, J.; Kim, Y. S.; Kim, Y. H.; Lee, J.-Y.; Bae, I. C.; Lee, S.-G.; Kim, J.-H. Comparison of Analytical Performance of I-Smart 300 and

https://doi.org/10.1021/acssensors.1c01720
ACS Sens. 2022, 7, 441−452

PHOx Ultra for the Accurate Determination of Pleural Fluid PH. *Practical Lab. Med.* **2019**, *14*, No. e00117.
(66) Soller, B.; Zou, F.; Prince, M. D.; Dubick, M. A.; Sondeen, J. L. Comparison of Noninvasive PH and Blood Lactate as Predictors of Mortality in a Swine Hemorrhagic Shock with Restricted Volume Resuscitation Model. *Shock* **2015**, *44*, 90.
(67) Kurebayashi, N.; Harkins, A. B.; Baylor, S. M. Use of Fura Red as an Intracellular Calcium Indicator in Frog Skeletal Muscle Fibers. *Biophys J.* **1993**, *64*, 1934.
(68) Katoh, D.; Hongo, K.; Ito, K.; Yoshino, T.; Kayama, Y.; Komukai, K.; Kawai, M.; Date, T.; Yoshimura, M. A Technique for Quantifying Intracellular Free Sodium Ion Using a Microplate Reader in Combination with Sodium-Binding Benzofuran Isophthalate and Probenecid in Cultured Neonatal Rat Cardiomyocytes. *BMC Res. Notes* **2013**, *6*, 1−7.
(69) Witkowska Nery, E.; Kundys, M.; Jeleń, P. S.; Jönsson-Niedziółka, M. Electrochemical Glucose Sensing: Is There Still Room for Improvement? *Anal. Chem.* **2016**, *88*, 11271−11282.
(70) Vonck, J.; Parcej, D. N.; Mills, D. J. Structure of Alcohol Oxidase from Pichia Pastoris by Cryo-Electron Microscopy. *PLoS One* **2016**, *11*, No. e0159476.
(71) JCDR—Diabetes mellitus, Emphysematous pyelonephritis, Hyperglycaemia, Ketosis, Non-compliance. https://jcdr.net/article_fulltext.asp?issn=0973-709x&year=2015&volume=9&issue=6&page=OC01&issn=0973-709x&id=5995 (accessed Nov 9, 2021).
(72) Andersen, L. W.; Mackenhauer, J.; Roberts, J. C.; Berg, K. M.; Cocchi, M. N.; Donnino, M. W. Etiology and Therapeutic Approach to Elevated Lactate Levels. *Mayo Clin. Proc.* **2013**, *88*, 1127−1140.
(73) Ibarra, G.; Majmundar, M. M.; Pacheco, E.; Zala, H.; Chaudhari, S. Hypernatremia in Diabetic Ketoacidosis: Rare Presentation and a Cautionary Tale. *Cureus* **2020**, *12* (). DOI: 10.7759/CUREUS.11841.
(74) Castellanos-Mendoza, A.; Castro-Acosta, R. M.; Olvera, A.; Zavala, G.; Mendoza-Vera, M.; García-Hernández, E.; Alagón, A.; Trujillo-Roldán, M. A.; Valdez-Cruz, N. A. Influence of PH Control in the Formation of Inclusion Bodies during Production of Recombinant Sphingomyelinase-D in Escherichia Coli. *Microb. Cell Fact.* **2014**, *13*, 1−14.
(75) Marles, R. J. Mineral Nutrient Composition of Vegetables, Fruits and Grains: The Context of Reports of Apparent Historical Declines. *J. Food Compos. Anal.* **2017**, *56*, 93−103.
(76) Zulkifli, S. N.; Rahim, H. A.; Lau, W.-J. Detection of Contaminants in Water Supply: A Review on State-of-the-Art Monitoring Technologies and Their Applications. *Sens. Actuators, B* **2018**, *255*, 2657−2689.
(77) Thakur, M. S.; Ragavan, K. v. Biosensors in Food Processing. *J. Food Sci. Technol.* **2013**, *50*, 625−641.

https://doi.org/10.1021/acssensors.1c01720
ACS Sens. 2022, 7, 441−452